Malaysian Journal of Catalysis 9 (2025) 22-30

Malaysian Journal of Catalysis
http://mjcat.utm.my/

MJCat
Research Article

# Enhancing Nickel-Based Catalysts for Hydrodeoxygenation: The Role of Sulfated and Phosphated Silica Supports

Fadli Rosyad[1,2], Sri Wahyuni[2], Egi Agustian[1], Adid Adep Dwiatmoko[1]*, Yati Maryati[1], Nino Rinaldi[1], Robert Ronal Widjaya[1], Anis Kristiani[1] and Avga Spica[1,3]

[1] *Research Center for Chemistry, National Research and Innovation Agency (BRIN), Tangerang Selatan, Indonesia.*
[2] *Department of Chemistry, Faculty of Mathematics and Natural Sciences, Universitas Negeri Semarang, Semarang, Indonesia.*
[3] *Department of Chemistry, Faculty of Mathematics and Natural Sciences, Universitas Indonesia, Depok, Indonesia.*

**Corresponding Author: adid001@brin.go.id*

*Article history:*
*Received 20 November 2024*
*Accepted 21 January 2025*

ABSTRACT

The development of efficient catalysts for hydrodeoxygenation (HDO) is crucial for producing sustainable hydrocarbons from biomass-derived feedstocks. In this investigation, silica ($SiO_2$) supports were modified through sulfation and phosphatization treatments to enhance the performance of nickel-based catalysts for HDO reactions. The modified silica supports, $SiO_2$-S (sulfated) and $SiO_2$-P (phosphated), were characterized using XRD, FTIR, $N_2$ physisorption, and FE-SEM techniques to assess their structural changes, surface area, and nickel dispersion. $SiO_2$-S exhibited the lowest surface acidity and pore volume; however, it showed superior nickel dispersion and smaller particle sizes. The catalytic performance was evaluated in HDO reactions, with Ni/$SiO_2$-S achieving the highest hydrocarbon selectivity (89.3%), particularly for C17 hydrocarbons, attributed to the replacement of hydroxyl group on the silica surface with sulfate groups. Ni/$SiO_2$-P also improved hydrocarbon production compared to untreated $SiO_2$, albeit with lower selectivity. This research elucidates the critical role of support modification in optimizing nickel-based catalysts for HDO reactions.

*Keywords*: *Oleic Acid, hydrodeoxygenation, Acid treatment, Silica, Ni/$SiO_2$*


| eISSN 0128-2581

## 1. INTRODUCTION

The global consumption of fuel oil has increased significantly owing to population growth and expansion of the market economy. Among various fuels, gasoline is the most widely used. It is derived from fossil materials, primarily formed from ancient plants and animals. However, fossil fuels are finite resources, and their continuous use could lead to depletion and disruption of the global fuel supply, especially for vehicles that rely heavily on them[1]. One potential solution to this problem is the development and use of biofuel fuels derived from plants. As biofuels are renewable and non-fossil fuels, they offer the potential to replace conventional fossil fuels[2].

Biofuels can be synthesized from fatty acids via several reactions including catalytic cracking, hydrocracking, hydrogenation, and hydrodeoxygenation (HDO)[3]. HDO is an industrial process used to remove oxygen from compounds by saturating double bonds. In these processes, catalysts play a key role by accelerating the reaction and breaking down long-chain molecules into shorter ones, which facilitates faster and more efficient biofuel production. Nickel (Ni) metals are frequently used as active components in these catalysts because of their effectiveness as transition metals[4–7]. However, Ni is prone to deactivation and sintering, which can lead to an increase in particle size and a reduction in catalyst quality[8]. To counteract these issues, a suitable support material is required to stabilize Ni particles, maintain their surface area, and prevent sintering[9].

Silica ($SiO_2$) derived from rice husk ash is an excellent candidate catalyst support. Rice husk ash, a byproduct of rice husk combustion, contains up to 96% $SiO_2$[10]. It has a high surface area and high thermal stability, making it an ideal support material for catalysts. Catalyst activity, which is a measure of catalyst performance, depends on several factors, including surface area and acidity.

Acid treatment of catalyst supports can further enhance their activity. For example, Sekewael et al. (2022) demonstrated that sulfated $ZrO_2$ catalysts achieved a conversion rate of 93% compared with 77% for untreated $ZrO_2$[11]. This improvement was attributed to the increase in the surface area and acidity resulting from sulfation treatment. Similarly, acid-treated $SiO_2$-supported Ni catalysts are expected to perform well for the production of

biofuels from oleic acid. Ni readily forms coordinate covalent bonds, facilitating the formation of intermediate compounds on the catalyst surface, which enhances the hydrodeoxygenation process.

Despite significant research on Ni-based catalysts and the benefits of acid-treated supports, there is limited understanding of the specific impact of different acid treatments on the structural and catalytic properties of rice-husk-ash-derived $SiO_2$-supported Ni catalysts. Additionally, there is a lack of comprehensive studies comparing the performance of these catalysts in the hydrodeoxygenation of oleic acid to that of other fatty acids.

This study aims to utilize the high $SiO_2$ content of rice husk ash as a catalyst support and synthesize $Ni/SiO_2$ catalysts to convert oleic acid into hydrocarbons suitable for biofuel production. Oleic acid, a fatty acid commonly found in vegetable oils, such as olive oil (55-80%), palm oil (38.4%)[12], sunflower oil (11.7%)[13], and grape seed oil (15%), is a promising feedstock for biofuel production. Thus, Ni catalysts can effectively convert oleic acid into hydrocarbon compounds, which can be used as biofuels. By enhancing the catalyst support through acid treatment, catalytic activity can be improved, leading to higher biofuel yields.

## 2. EXPERIMENTS

### 2.1 Isolation of $SiO_2$ from Rice Husk Ash

To isolate the $SiO_2$, 20 g of rice husk ash was dispersed in 100 mL of 2 M HCl and stirred for 6 h. The resulting mixture was vacuum filtered, and the solid residue was collected. The residue was then dried in an oven at 100 °C. The dried solid was then mixed with 100 mL of 2.5 M NaOH solution and stirred at 90 °C for 3 h to dissolve the silica. After filtration, the residue was washed with warm water. The resulting filtrate containing sodium silicate ($Na_2SiO_3$) was cooled to room temperature and left to stand overnight. To precipitate silica, the sodium silicate solution was titrated with 5 M $H_2SO_4$ under constant magnetic stirring. The titration was carefully controlled to induce the formation of white gelatinous silica gel. The gel was thoroughly washed with water until the pH of the washing solution reached neutrality. Finally, the silica gel was dried at 105 °C for 15 h to obtain the solid $SiO_2$.

### 2.2. Catalyst Preparation

#### 2.2.1. Sulfated-$SiO_2$

In this step, 20 mL of acetone and 2 mL of $H_2SO_4$ were combined in an Erlenmeyer flask (Solution A). Separately, 12 g of $SiO_2$ derived from rice husk ash was immersed in 72 mL acetone. The immersed $SiO_2$ was then added to Solution A stirred for 4 h. The resulting solution was filtered, and the obtained solid was washed multiple times with distilled water to remove any excess acid. The washed solid was dried in an oven at 100 °C for 24 h to produce $SiO_2$ ($SiO_2$-S).

#### 2.2.2. Phosphated-$SiO_2$

For phosphatizing, 20 mL of acetone and 2 mL $H_3PO_4$ were mixed in an Erlenmeyer flask (Solution B). Simultaneously, 18 g of $SiO_2$ from rice husk ash was added to 108 mL of acetone. The mixture was then added to Solution B and stirred for 4 h. The mixture was filtered and the solid was thoroughly washed with distilled water to remove excess acid. The washed solid was dried in an oven at 100 °C for 24 h to yield phosphated $SiO_2$ ($SiO_2$-P)

#### 2.2.3. $Ni/SiO_2$ Catalyst

For the synthesis of the $Ni/SiO_2$ catalyst, 2.97 g of $Ni(NO_3)_2 \cdot 6H_2O$ was dissolved in 20 mL of distilled water in a 100 mL Erlenmeyer flask. To this solution, 5.4 g of $SiO_2$ was added to this solution and the mixture was refluxed on a hotplate with continuous stirring for 24 h. The mixture was dried at 90 °C and calcined at 450 °C for 2 h. Finally, the catalyst was reduced at 450 °C for 4 h to obtain $Ni/SiO_2$.

### 2.3. Catalyst characterizations

The crystal structure of the catalyst was analyzed using XRD with a PANalytical Empyrean instrument with monochromatic radiation CuKα (λ = 1.54056 Å). The XRD analysis was conducted within a scanning range of 5–90° at a rate of 10°/min with a step width of 0.02°. The morphologies and elemental analysis of the samples were characterized by scanning electron microscopy (SEM)-energy dispersive X-ray (EDX) using an SEM Hitachi SU3500. $N_2$-physisorption was obtained using a Micromeritics TriStar II 3020. The catalyst acidity was analyzed by the ammonia temperature-programmed desorption ($NH_3$-TPD) method using a Micromeritics Chemisorb 2750. All samples were pretreated in helium gas flow for 30 min at 350 °C and exposed to flowing diluted ammonia gas at 40 mL/min for 30 min at 100 °C. It was then purged with helium gas flow for 30 min at 100 °C to remove physically adsorbed ammonia. Subsequently, the sample was heated to 800 °C at a rate of 10 °C/min.

### 2.4. Catalytic reaction

The performance of $Ni/SiO_2$ as a catalyst was assessed by HDO using oleic acid in a batch reactor. The reaction setup involved placing 1 g of $Ni/SiO_2$ catalyst and 10 mL of oleic acid into the reactor, which was then securely positioned within a heating furnace. Before initiating the reaction, the system was subjected to a thorough leak check. Once leak-free, hydrogen gas ($H_2$) was introduced into the reactor at a pressure of 40 bar. The reactor temperature was

then increased to 350 °C and the reaction proceeded under these conditions for 2 h.

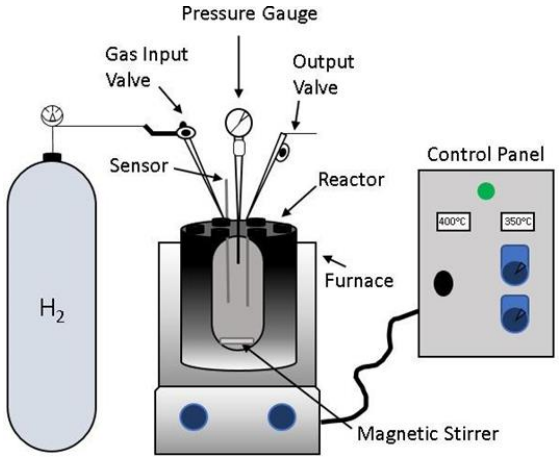


**Schematic 1.** Batch reactor setup for hydrodeoxygenation

## 3. RESULTS AND DISCUSSION

Sulfation and phosphatization treatments are commonly used to modify silica ($SiO_2$), making it more reactive and increasing its surface area. Sulfation involves the reaction of silica with sulfuric acid ($H_2SO_4$), which results in the protonation of silica and the release of hydroxyl ions ($OH^-$). The reaction can be represented as:

$$SiO_2 + H_2SO_4 \rightarrow Si\text{-}OH + HSO_4^-$$

In this process, the protonation of silica generates silanol groups (Si-OH), which are more reactive. Similarly, phosphatization involves the reaction of silica with phosphoric acid ($H_3PO_4$), producing reactive silanol groups via a comparable mechanism:

$$SiO_2 + H_3PO_4 \rightarrow Si\text{-}OH + H_2PO_4^-$$

Based on the XRD patterns presented in Figure 1A, the diffraction patterns of $SiO_2$-P, $SiO_2$-S, and $SiO_2$ reveal broad diffraction peaks at approximately $2\theta = 22°$, which is consistent with the characteristic amorphous silica pattern[14]. In contrast, the XRD patterns of Ni/$SiO_2$, Ni/$SiO_2$-P, and Ni/$SiO_2$-S in Figure 1b show sharp peaks at approximately $2\theta = 44.38°$, 51.73°, and 76.30°, respectively, which are indicative of the crystalline phases of metallic nickel (Ni). These peaks correspond to the (111), (200), and (220) planes of face-centered cubic (fcc) +Ni[15], indicating the presence of highly ordered crystalline Ni on the silica supports. The slight shifts in the $2\theta$ values of the Ni/$SiO_2$, Ni/$SiO_2$-P, and Ni/$SiO_2$-S samples can be attributed to variations in the interaction between the Ni nanoparticles and different $SiO_2$ supports resulting from the acid treatments applied to the silica. These treatments, such as sulfation and phosphatization, appear to slightly affect the crystalline structure of the Ni phase, suggesting that the surface modification of silica influences the degree of crystallinity and the interaction between Ni particles and the $SiO_2$ surface, which may affect the catalytic performance of the materials[16].

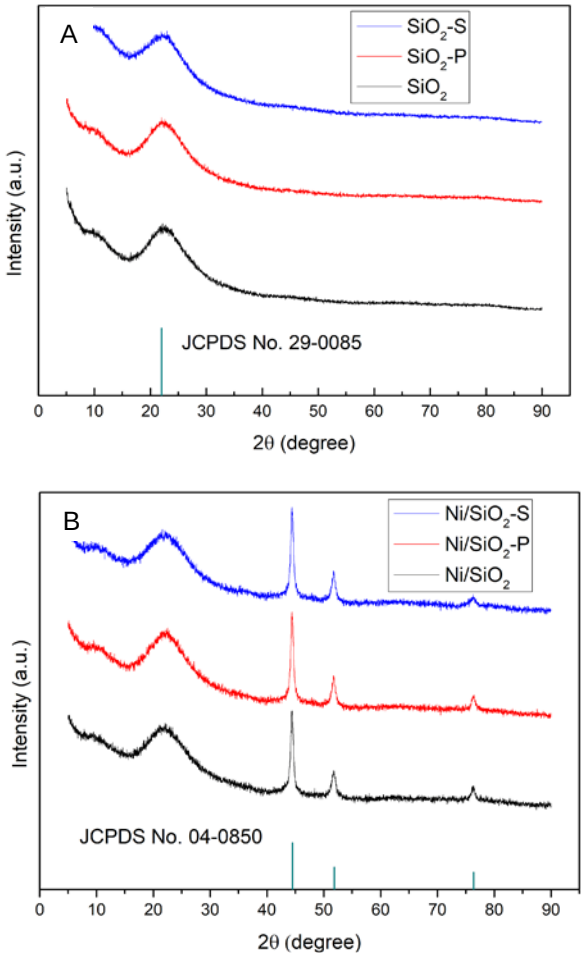


**Figure 1.** XRD pattern of the samples: (A) $SiO_2$ and (B) Ni/$SiO_2$

Figure 2 shows the FTIR spectra of the $SiO_2$ support. This provides important insights into the chemical composition of $SiO_2$. Several characteristic absorption bands corresponding to specific functional groups are observed, indicating the successful formation of $SiO_2$ and the presence of modifications in $SiO_2$-P and $SiO_2$-S. The absorption band around 3375 $cm^{-1}$ is associated with the O-H stretching vibration, which is attributed to hydroxyl (-OH) groups, commonly referred to as silanol groups (Si-OH)[17]. This band is particularly significant because it indicates the presence of Brønsted acid sites, which contribute to the surface acidity of $SiO_2$[18,19]. Among the three samples, $SiO_2$-P showed the lowest transmittance at this wavenumber,

suggesting that phosphatization led to a reduction in hydroxyl groups, potentially owing to the formation of phosphate species on the surface. $SiO_2$-S shows a slightly higher transmittance than $SiO_2$-P, but is still lower than that of unmodified SiO2, indicating that sulfation also affects the concentration of hydroxyl groups on the surface. The strong band observed at approximately 1056 $cm^{-1}$ corresponds to the asymmetric stretching vibration of the Si-O-Si bond, which is characteristic of siloxane groups[20]. This band was present in all the three samples, confirming the successful formation of the $SiO_2$ framework. This confirmed the presence of $SiO_2$ as the primary component in the samples. The transmittance values remained consistent across all the samples, suggesting that the siloxane network remained intact even after the phosphatization and sulfation treatments. The band at 1599 $cm^{-1}$ corresponds to the bending vibration of Si-O bonds, which also contributes to the structural integrity of the siloxane (Si-O-Si) network[21]. The presence of this band in all samples indicates that the $SiO_2$ backbone was preserved across the different modifications. There were no significant shifts or changes in this band, indicating that the structural changes mainly involved surface functional groups.

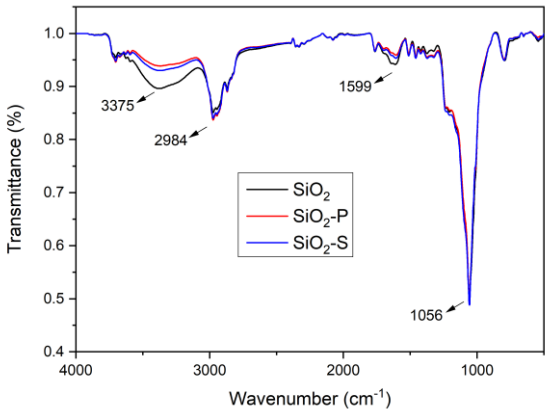


**Figure 2.** FTIR spectrum of $SiO_2$

The $N_2$ physisorption data of the $SiO_2$ samples, including untreated silica ($SiO_2$), phosphated silica ($SiO_2$-P), and sulfated silica ($SiO_2$-S), revealed significant differences in surface area, pore diameter, and pore volume owing to the varying chemical treatments and nickel impregnation. Table 1 shows that untreated silica ($SiO_2$) has a surface area of 194.7 $m^2/g$, a pore diameter of 10.37 nm, and a pore volume of 0.492 $cm^3/g$. After the phosphate (P) and sulfate (S) treatments, both $SiO_2$-P and $SiO_2$-S showed considerable changes. $SiO_2$-P exhibited the highest surface area of 263.5 $m^2/g$ and a substantial increase in pore volume (0.945 $cm^3/g$). This suggests that phosphate treatment induces additional porosity and a greater mesoporous structure, likely owing to the formation of new pore channels or increased textural porosity[22], resulting in a higher surface area and pore volume[23], as observed from the slight increase in the pore diameter of $SiO_2$-P (13.75 nm) compared with that of untreated $SiO_2$. In contrast, $SiO_2$-S displays a lower surface area (135.1 $m^2/g$), pore volume (0.502 $cm^3/g$), and an increased pore diameter (13.24 nm), indicating that the sulfate treatment leads to pore expansion but reduces overall surface area, possibly due to the partial blockage of pores or restructuring caused by the acid treatment[24]. Sulfate treatment tends to block some pores owing to the strong interactions with sulfate groups, which can reduce the overall surface area while slightly expanding the remaining pores. Additionally, it may decrease the textural properties by altering the pore network structure. Thus, the chemical nature of these anions significantly influences the modification of $SiO_2$[25].

**Table 1.** Physical and chemical properties of prepared catalysts

| Samples | Surface Area ($m^2/g$) | Pore diameter (nm) | Pore volume (cm3/g) | Total acidity (mmol/g) |
|---|---|---|---|---|
| $SiO_2$ | 194.7 | 10.37 | 0.492 | 1.079 |
| $SiO_2$-S | 135.1 | 13.24 | 0.502 | 0.091 |
| $SiO_2$-P | 263.5 | 13.75 | 0.945 | 0.975 |
| Ni/$SiO_2$ | 106.3 | 14.35 | 0.740 | - |
| Ni/$SiO_2$-S | 90.2 | 15.26 | 1.013 | - |
| Ni/$SiO_2$-P | 127.8 | 15.71 | 0.760 | - |

The total acidity, as shown in Table 1, exhibited a notable trend: $SiO_2$ demonstrated the highest total acidity (1.079 mmol/g), which decreased substantially in $SiO_2$-S (0.091 mmol/g), indicating that sulfation significantly reduced the number of acidic sites, potentially due to the modification of acid sites during the sulfation process. In contrast, phosphate treatment resulted in a moderate acidity value of 0.975 mmol/g, suggesting that while phosphate treatment reduces acidity compared to pure $SiO_2$, it does not do so as extensively as sulfation. The reduction in acidity observed after sulfation and phosphate treatment can be attributed to alterations in the surface chemistry of $SiO_2$. In the case of sulfation, sulfate groups ($SO_4^{2-}$) are introduced onto the silica surface, which interact with surface hydroxyl groups (Si–OH), neutralizing some of the Brønsted acidic sites responsible for the material's acidity. This process modifies the surface structure and decreases the number of available acidic sites, as the sulfate groups are less acidic than the Si–OH groups, leading to a significant reduction in the total acidity. Similarly, phosphate treatment involves the introduction of phosphate groups ($PO_4^{3-}$) onto the silica surface, which can passivate the surface by interacting with hydroxyl groups and reducing the number of acidic sites. In both cases, modification of the surface and neutralization or replacement of acid sites with less acidic species resulted in a decrease in total acidity.

The pore size distribution graph in Figure 3A highlights these effects, with $SiO_2$-P demonstrating a higher

differential surface area across various pore widths, confirming the generation of additional mesopores or an enhancement in the connectivity of the porous network. $SiO_2$-S showed a more limited increase in mesopore volume, consistent with the moderate increase in pore diameter and relatively lower surface area. $SiO_2$-P exhibits a higher differential surface area across various pore widths than $SiO_2$-S owing to the formation of new mesopores and enhanced connectivity within the porous network. This increased accessibility allows for greater interaction with adsorbates, whereas sulfate treatment may block or partially occlude pores, limiting gas adsorption. Additionally, phosphate treatment stabilizes the pore structure of $SiO_2$, preventing collapse, whereas sulfate modification can inhibit pore accessibility, contributing to the observed differences in the surface area[26].

The nitrogen adsorption-desorption isotherms in Figure 3B further confirm these observations. The step increases in the adsorption curve at high relative pressures ($P/P_o > 0.8$) for $SiO_2$-P suggested the presence of larger mesopores or macropores, which correlated with the high pore volume and surface area. $SiO_2$-S, while showing similar trends, adsorbed less nitrogen overall, implying fewer available mesopores and a lower capacity for gas adsorption. Figure 3c shows the pore size distributions of the Ni/$SiO_2$ catalysts. The graph shows that Ni/$SiO_2$-S exhibits the highest pore distribution peak around the pore range of 20-40 nm, which is consistent with the table data, indicating an average pore diameter of 15.26 nm. This suggests a significant increase in differential surface area. Meanwhile, Ni/$SiO_2$-P displayed a broader pore distribution compared to the other variants, reflecting a higher surface area (127.8 $m^2/g$) and a substantial pore volume (0.760 $cm^3/g$). This enhancement implies that the phosphate treatment improved the structure and connectivity of the pores. Furthermore, Figure 3d presents the nitrogen adsorption-desorption isotherms for the Ni/$SiO_2$ catalysts. Ni/$SiO_2$-P showed a higher adsorption curve across the relative pressure range, particularly at high pressures ($P/Po > 0.8$), indicating the presence of larger mesopores or macropores. This is consistent with its high pore volume and large surface area. In contrast, Ni/$SiO_2$-S exhibited lower nitrogen adsorption, suggesting that sulfate treatment may restrict the pore accessibility. Although the pore volume is higher (1.013 $cm^3/g$), the lower surface area (90.2 $m^2/g$) implies that pore accessibility might be hindered by the sulfate treatment. Ni/$SiO_2$ demonstrated a more linear isotherm, indicating a more uniform mesopore distribution with a significant average pore size and volume. These differences underscore the substantial impact of chemical modifications on the pore structure and adsorption-desorption properties of the materials.

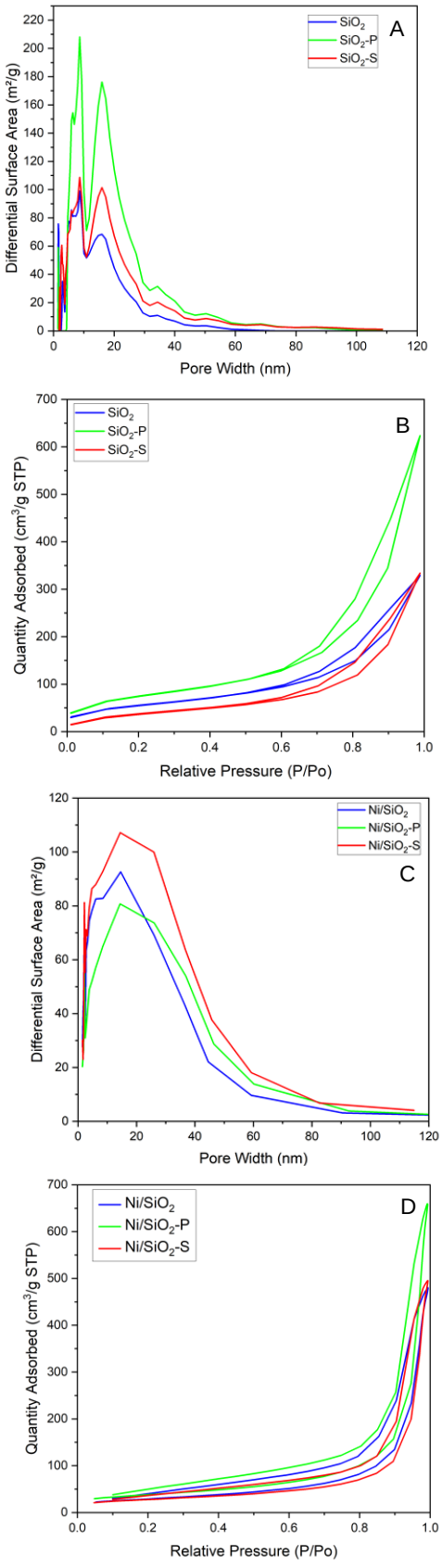

**Figure 3.** Pore size distribution and adsorption-desorption isotherm of $SiO_2$ (A, B) and $Ni/SiO_2$ (C, D)

Nickel impregnation significantly affected the surface properties of the $Ni/SiO_2$, $Ni/SiO_2$-S, and $Ni/SiO_2$-P samples. The surface areas of Ni-impregnated samples are consistently lower than their corresponding untreated counterparts, with $Ni/SiO_2$-P showing a surface area of 127.8 $m^2/g$ compared to 263.5 $m^2/g$ for $SiO_2$-P. This reduction is likely due to partial blockage of the pores by the nickel species. The pore diameters also increased slightly after Ni impregnation, suggesting that Ni deposition occurred primarily within the mesopores, expanding their size but reducing the surface area. The highest pore volume was observed for $Ni/SiO_2$-S (1.013 $cm^3/g$), reflecting enhanced mesoporosity, possibly due to changes in the silica structure induced by both sulfate and nickel.

Figure 4 displays the FESEM images and EDS analyses of $Ni/SiO_2$, $Ni/SiO_2$-S, and $Ni/SiO_2$-P, which provide valuable insights into the morphology, surface distribution, and nickel dispersion across the silica supports that have undergone acid treatment. These results reflect the impact of phosphate and sulfate acid treatments on the structural properties of silica and how these treatments influence the dispersion and particle size of Ni.

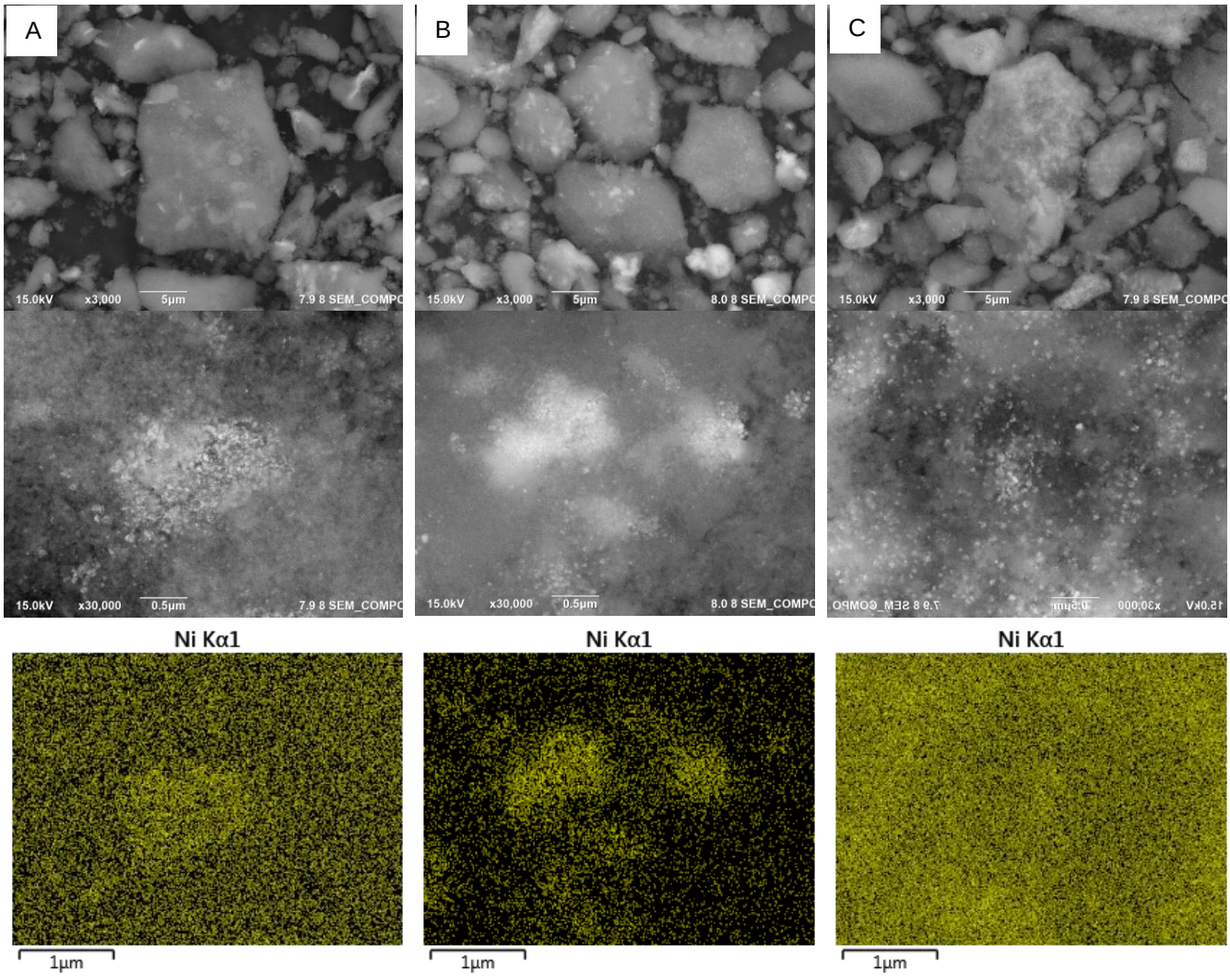


**Figure 4.** FESEM images and EDX analysis of $Ni/SiO_2$ (A), $Ni/SiO_2$-S (B) and $Ni/SiO_2$-P (C)

Significant differences in surface morphology were observed among the three samples. In the case of $Ni/SiO_2$ (Figure 4A), untreated silica exhibited relatively larger and more irregular particle aggregates. The surface presented a rough appearance with less uniformity in particle size. The EDS map of Ni Kα1 for $Ni/SiO_2$ revealed a reasonably even

distribution of nickel across the surface; however, the relatively lower magnification suggests that nickel particles may be present in larger clusters or agglomerates, potentially affecting the catalytic performance by reducing the active surface area and increasing the likelihood of sintering. In contrast, Ni/$SiO_2$-S (Figure 4B), where the silica support had undergone sulfate acid treatment, exhibited smaller, more defined particles, indicating restructuring of the silica surface due to the acid treatment. FE-SEM images at a higher magnification (30,000×) revealed finer Ni particles dispersed on the support. The EDS map demonstrated a highly homogeneous distribution of Ni, suggesting that sulfate treatment enhanced Ni dispersion. This enhancement was likely due to the sulfate groups anchoring the nickel species more effectively to the support, thus preventing the formation of larger nickel clusters[26]. The enhanced dispersion of Ni may also be attributed to the increased pore size observed in Ni/$SiO_2$-S, allowing better accessibility and uniform distribution of Ni throughout the mesopores. The phosphated silica (Figure 4C) support exhibited a morphology with small, well-distributed particles, similar to Ni/$SiO_2$-S, but with more significant textural differences. The FE-SEM image revealed more evenly dispersed smaller particles across the surface, and EDS mapping demonstrated a high concentration of nickel distributed evenly across the support. Phosphate treatment, similar to sulfate treatment, enhances Ni dispersion, albeit through a different mechanism. The phosphate groups may increase the surface acidity and facilitate a more favorable environment for the dispersion of nickel, potentially by forming stronger interactions between the nickel ions and phosphate-modified silica surface[23]. This results in a well-dispersed Ni phase, even at higher concentrations, preventing the agglomeration of large Ni particles.

The differences in Ni dispersion and particle size between these samples were strongly influenced by the acid treatments applied to the silica supports. Sulfate and phosphate treatments enhance nickel dispersion through different mechanisms. Sulfate treatment increases the pore size, providing better access for the uniform distribution of Ni ions, whereas phosphate treatment likely modifies the surface chemistry, enhancing the interaction between Ni and the support[25]. Additionally, the increase in the surface area and pore volume observed in the $N_2$ physisorption data for $SiO_2$-P supports the idea that phosphate treatment facilitates the uniform dispersion of nickel particles by providing a larger available surface and a more porous structure.

The GC-MS data presented in Figure 5 elucidate the influence of catalyst support modification on hydrocarbon selectivity during the hydrodeoxygenation reaction. Despite the fact that the majority of the product in our reaction is in the solid form, Figure 5A demonstrates that Ni/$SiO_2$-S exhibits the highest hydrocarbon selectivity (89.3%), followed by Ni/$SiO_2$-P (64.9%) and Ni/$SiO_2$ (56.5%). The sulfated silica catalyst demonstrated superior performance, indicating that the incorporation of sulfate groups significantly enhanced the production of hydrocarbons, while suppressing the formation of fatty acids, alcohols, and other oxygenated compounds. The high hydrocarbon selectivity of Ni/$SiO_2$-S can be attributed to the siloxane groups created by the sulfation process. These groups facilitate the hydrodeoxygenation pathway, leading to a more complete deoxygenation and higher selectivity towards hydrocarbons. Conversely, Ni/$SiO_2$-P, with moderate acidity from the phosphate groups, also performed well but did not reach the same level of hydrocarbon production as Ni/$SiO_2$-S. Untreated $SiO_2$, which lacks significant functional groups, displayed the lowest hydrocarbon selectivity and a higher presence of fatty acids and alcohols, suggesting less effective deoxygenation.

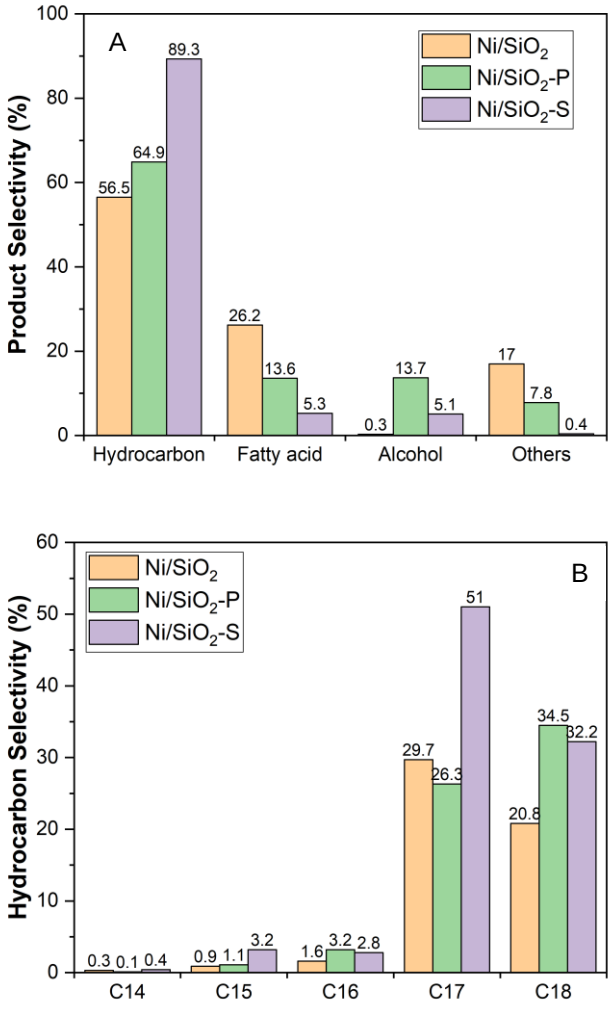


**Figure 5.** Product selectivity after the reaction

Figure 5B shows the detailed hydrocarbon selectivity by carbon chain length (C14–C18); further insights were gained into the distribution of products. Ni/$SiO_2$-S showed the highest selectivity for C17 hydrocarbons (51%), followed by Ni/$SiO_2$-P (26.3%), and Ni/$SiO_2$ (29.72%). For

C18 hydrocarbons, $Ni/SiO_2$-P displayed the highest selectivity (34.49%), followed closely by $Ni/SiO_2$-S (32.21%), and $Ni/SiO_2$ (20.78%). These results confirm that both $Ni/SiO_2$-S and $Ni/SiO_2$-P support the production of longer-chain hydrocarbons (C17 and C18), which are typically desirable for hydrodeoxygenation reactions, especially for producing diesel-range fuels.

The superior performance of $Ni/SiO_2$-S is believed to be linked to its enhanced siloxane functional groups, which promote catalytic cracking and hydrodeoxygenation, favoring the formation of longer-chain hydrocarbons[25]. Phosphated silica ($Ni/SiO_2$-P) also enhances catalytic activity compared to untreated $SiO_2$, but its lower acidity results in less efficient cracking and HDO compared to $Ni/SiO_2$-S. This also explains why $Ni/SiO_2$-P favors the formation of C18 hydrocarbons slightly more than C17, as the acidity may not be strong enough to break down the larger molecules into smaller fractions.

The $Ni/SiO_2$ catalyst, which lacks surface functional groups owing to the absence of sulfate or phosphate groups, shows a more balanced selectivity for C17 and C18, but generally lower hydrocarbon production. It is possible that poorer metal dispersion on the untreated $SiO_2$ support reduced the efficiency of the HDO process, leading to higher amounts of oxygenated compounds such as fatty acids and alcohols, as shown in the first figure. Nickel dispersion and particle size play crucial roles in the catalytic performance. The impregnation of nickel on sulfated and phosphated silica likely leads to better dispersion and smaller particle sizes, owing to the stronger interaction between the acidic support and nickel. This resulted in a higher number of active sites, which increased the catalytic efficiency and selectivity for hydrocarbons. In contrast, nickel on untreated silica may be less well dispersed, resulting in larger particles, fewer active sites, and therefore, lower catalytic activity.

The differences in hydrocarbon selectivity and product distribution across the $Ni/SiO_2$, $Ni/SiO_2$-S, and $Ni/SiO_2$-P catalysts can be explained by variations in surface acidity, nickel dispersion, and particle size. The strong acidity introduced by the sulfate groups in $Ni/SiO_2$-S dramatically improves hydrocarbon selectivity, particularly for C17 and C18 hydrocarbons, making it the most efficient catalyst in this study. Phosphated silica ($Ni/SiO_2$-P) also improves the catalytic performance compared to untreated silica, but to a lesser extent because of its moderate acidity. The untreated silica support ($Ni/SiO_2$) had lower hydrocarbon selectivity and higher oxygenated compound production, reflecting the lack of sufficient acidic sites and poor nickel dispersion.

## 4. CONCLUSION

The modification of silica with sulfate ($SiO_2$-S) and phosphate ($SiO_2$-P) significantly enhances the catalytic performance of $Ni/SiO_2$ catalysts in hydrodeoxygenation reactions, with $Ni/SiO_2$-S demonstrating the highest hydrocarbon selectivity (89.3%) owing to its chemical surface. The sulfation process improved nickel dispersion, pore structure, and acidity, resulting in superior selectivity for C17 hydrocarbons. $Ni/SiO_2$-P also increased the catalytic efficiency but exhibited lower hydrocarbon selectivity than $Ni/SiO_2$-S, which was attributed to its moderate acidity. $Ni/SiO_2$ displayed lower hydrocarbon production and higher oxygenated by-products, underscoring the critical role of support modification in enhancing the catalytic performance.

## ACKNOWLEDGEMENTS

This work was supported by the Korea Institute of Science and Technology (KIST) through the KIST Alumni Project 2024, and the National Research and Innovation Agency (BRIN) through the RPORNM 2024 program.

## REFERENCES

[1] A.N. Aini, M. Al-Muttaqii, A. Roesyadi, F. Kurniawansyah, (2021) 149–156.
[2] N. Rodiansono, H.P. Dewi, K. Mustikasari, M.D. Astuti, S. Husain, N. Sutomo, (2022) 13319–13329.
[3] A.A. Dwiatmoko, I. Kim, L. Zhou, J. Choi, D. Suh, J. Jae, J. Ha, (2017).
[4] I. Aziz, P. Sugita, N. Darmawan, A.A. Dwiatmoko, (2023).
[5] Y. Liu, L. Yao, H. Xin, G. Wang, D. Li, C. Hu, (2015) 504–514.
[6] F.I. Prihadiyono, W.W. Lestari, R. Putra, A.N.L. Aqna, I.S. Cahyani, G.T.M. Kadja, (2022) 931–931.
[7] R. Riyandi, N. Rinaldi, R.T. Yunarti, A.A. Dwiatmoko, F.S.H. Simanjuntak, (2024).
[8] P. Strucks, L. Failing, S. Kaluza, (2021) 1526–1536.
[9] X. Gao, Z. Ge, G. Zhu, Z. Wang, J. Ashok, S. Kawi, (2021) 1003.
[10] V.H. Le, C. Nhan, H. Thuc, H.H. Thuc, (2013) 1–10.
[11] S.J. Sekewael, R.A. Pratika, L. Hauli, A.K. Amin, M. Utami, K. Wijaya, (2022).
[12] M. Bahadi, N. Salih, J. Salimon, (2021) 175–186.
[13] S. Shabrina, R.TD.W. Broto, (2023) 1–4.
[14] H.F. Poulsen, J. Neuefeind, H.B. Neumann, J.R. Schneider, M.D. Zeidler, (1995) 63–74.
[15] I. Rossetti, A. Gallo, V. DalSanto, C.L. Bianchi, V. Nichele, M. Signoretto, E. Finocchio, G. Ramis, A. Di Michele, (2013) 294–306.
[16] K.D. Ghuge, A.N. Bhat, G.P. Babu, (1993) 183–204.
[17] I. Zuwanna, M. Riza, S. Aprilia, Y. Syamsuddin, R. Dewi, (2023) 337–343.
[18] M.L. Hair, (1975) 299–309.

[19] C. Carteret, (2009) 13300–13308.
[20] J.M. Zeigler, F.W.G. Fearon, eds., (1989).
[21] J. Lewandowska-Łańcucka, M. Staszewska, M. Szuwarzyński, S. Zapotoczny, M. Kepczynski, Z. Olejniczak, B. Sulikowski, M. Nowakowska, (2018) 57–68.
[22] L. Krösi, S. Papp, S. Beke, A. Oszkó, I. Dékány, (2010) 79–86.
[23] W. Huang, Y. Zhang, D. Li, (2017) 470–482.
[24] N. Asasian Kolur, S. Sharifian, T. Kaghazchi, (2019) 663–675.
[25] V. Hegde, P. Pandit, P. Rananaware, V.P. Brahmkhatri, (2022) 1198–1210.
[26] Y. Wei, W. Yang, Z. Yang, (2022) 9537–9565.